# A Fuzzy Supervisory Scalar Control for Matrix Converter Induction Motor Drives

Mentari Putri Jati[1], Era Purwanto[2], Bambang Sumantri[3], Muhammad Rizani Rusli[4], Aris Nasuha[5], Anang Tjahjono[6] and Taufik Taufik[7]

[1.5]Electronic and Information Engineering Department, Universitas Negeri Yogyakarta, Indonesia
[2.3.6]Electrical Engineering Department, Politeknik Elektronika Negeri Surabaya, Indonesia
[4]Research and Development Department, PT. Garda Energi Nasional Indonesia, Sidoarjo, Indonesia
[7]Electrical Engineering Department, Cal Poly State University, San Luis Obispo, USA
mentariputrijati@uny.ac.id, era@pens.ac.id, bambang@pens.ac.id, ruslirizani@gmail.com, arisnasuha@uny.ac.id, anang.tj@pens.ac.id, taufik@calpoly.edu

*Abstract:* The dynamic performance of speed control of an induction motor has been known to be very sensitive to unavoidable disturbances such as unbalanced input supply and variable load torque. The effect on the controller performance further impacts the dynamic speed response and Total Harmonics Distortion (THD) of the system. Having a speed controller with good dynamic performance response, reliable handling of disturbances, high system efficiency, and low THD values is crucial in induction motor drives but challenging to accomplish. A matrix converter could potentially address the issues due to its reliability and efficient properties. In this paper, the Fuzzy Supervisory Controller (FSC) is embedded in a scalar control matrix converter fed induction motor drive with Indirect Space Vector Modulation (ISVM) to produce a reliable control system with improved dynamic performance. Reliability is evaluated by introducing voltage imbalance on the input and output sides of the motor drive. Based on the results of this work, the proposed controller can produce reliable speed control with good dynamic performance, work well under disturbances, and minimize current and voltage THD levels.

*Keywords*: matrix converter; induction motor; fuzzy supervisory scalar control

## 1. Introduction

Induction motors continue to be an interesting topic that attracts many researchers and practitioners around the globe due to their prevalent uses in industrial applications as well as electric vehicles [1], [2]. Issues that are often discussed in induction motor research include controller response performance improvement, disturbance rejection capability, power quality enhancement, and power electronic drive method. For the power electronic aspect of the induction motor drives, there are several important criteria such as high-efficiency, provision of 4-quadrant motor operation, and ability to mitigate various disturbances [3], [4]. Induction motors generally operate with a three-phase system which inherently has several types of disturbances that can interfere with the performance of control systems and drives. These include unbalanced input and output voltages [5], unbalanced output loads [6], nonlinear loads [7], differences in input and output frequencies [8], circuit switch failures [9], and non-sinusoidal waveform distortion on the input or output side [10]. Therefore, when designing a reliable induction motor drive system, all non-ideal conditions should inarguably be taken into consideration

When controlling the speed of an induction motor, the performance of the speed controller will not only greatly affect the dynamic response performance, but it will also influence the harmonic content of the motor drive system [11]. The variation of Total Harmonic Distortion (THD) values are an indirectly effect of speed control techniques that used in induction motor drive. The correlation between speed control and THD values begin with the stator current compiler with the $\alpha\beta$ reference frame, which is highly dependent on the rotor angular velocity ($\omega r$) [12], while the formulation of current THD is composed of the magnitude of the stator current value. The harmonic content of the motor drive system may reduce the supplying electric power system power quality which may further have very dangerous consequences [13].

Received: January 29th, 2021. Accepted: March 28th, 2021
DOI: 10.15676/ijeei.2021.13.1.12

Among power electronic converters used for induction motor drives, matrix converters have been known to have simple but robust hardware on the supply and load sides. The matrix converter with the vector modulation method offers the benefits of reducing the output current ripple [14], ability to select appropriate vectors based on reference voltage and current [15], eliminating commutation switch faults [16], providing power factor close to unity [17], improving voltage transfer ratio [18], reducing losses in switching devices [19], and operating in four quadrants [20]. This method could also be used for speed regulation applications. However, because the variable voltage frequency is determined by a single-stage conversion switch causing this method to have high complexity. In induction motor speed regulation applications, matrix converters require constant changes in the frequency and voltage ratio (scalar control) [21], [22]. This technique is the simplest, most powerful, easiest to use, and effective.

Despite the ability of the conventional control system to work well for the speed regulation of induction motors [23]. However, it suffers from the drawback of having constant control variables even when the operating system parameters change [24]. To overcome this issue, another controller was studied and developed that functions as a conventional control supervisor based on plant characteristics with the task of manipulating multivariable input and output to suit changes in the controlled plant. The study further implicates that the combination of fuzzy logic control and proportional-integral (PI) control into FSC will provide an improved solution.

Based on the aforementioned studies, this paper discusses the FSC control system application for matrix converter in induction motor speed drives which can span four operating quadrants, diminish THD value, and can provide reliability by overcoming supply and load disturbances. The overall work is done on the MATLAB Simulink platform to test and validate the proposed induction motor drive system.

## 2. Matrix Converter Drives

*A. Topology*

The nine switch matrix topology (3x3) is the basic topology of the matrix converter that connects the three-phase voltage source from the grid to the load of the three-phase induction motor. Two-way power flow by directly connecting the system input and output voltages as illustrated in Figure 1 [25]. The switching determination is determined from the bidirectional switch configuration in the hardware and can be used to determine the power losses of the converter. The configuration that is often used is the common emitter. The power losses mainly consist of switching and conduction losses of IGBT/MOSFET and diodes.

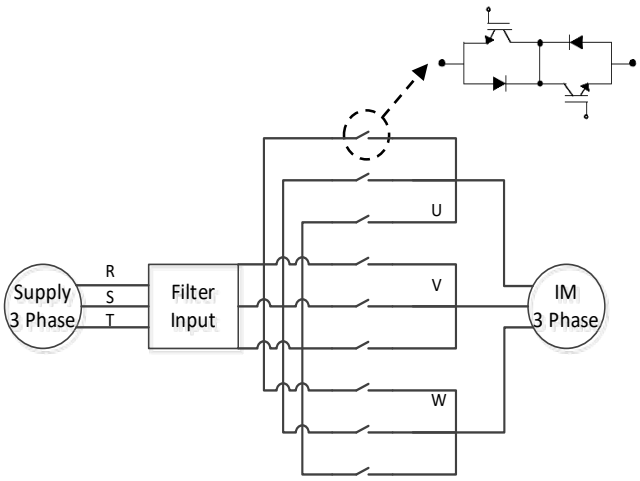


Figure 1. Input Filters Built into Bidirectional Three-Phase Matrix Converter Topology.

AC to DC conversion (rectifier) and DC to AC conversion (inverter) are elements of the two-stage AC to AC conversion in conventional methods. Changing DC waveform to AC waveform is easier than changing AC waveform and frequency to a different waveform and frequency being the cause of this method being widely used. The two-stage method, however, translates to larger losses than the one-stage counterpart due to the losses generated from the two converters.

*B. Indirect Space Vector Modulation*

The Space Vector Modulation (SVM) is the technique used to control the switching combination in the matrix converter. Another technique called the ISVM is defined as an equivalent circuit that combines a current source rectifier and a Voltage Source Inverter (VSI) connected via a virtual DC link as illustrated in Figure 2. The inverting stage has six switches as is a typical three-phase voltage source topology, S7 to S12, and the level rectifier has the same power topology as the other six switches, S1 to S6. The possible states of the switch and the appropriate current and voltage space vectors are determined based on the 27 switches combinations.

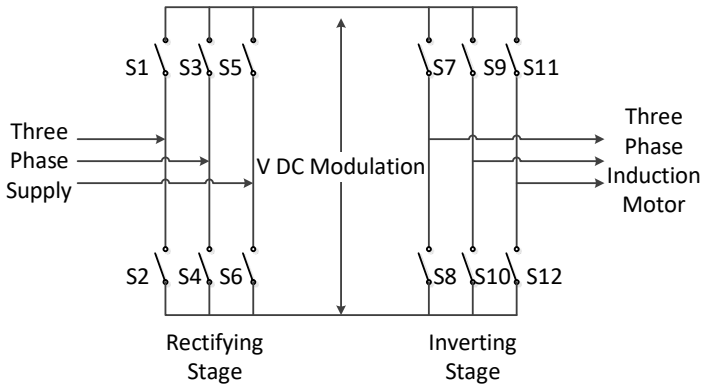


Figure 2. Equivalent Circuit of ISVM

The input voltage vector processes the three-phase output voltage of the matrix converter, while the output current vector processes the input current setting. The magnitude of the three phases is transformed into the $\alpha\beta$-axis which is used to calculate the amplitude of $|\ mag\ |$ and the reference angle $\theta$. Whereas, the amplitude $|\ mag\ |$ and the reference angle $\theta$ are separated into 6 vectors of voltage and current. The determination of the value and angle of a sector is calculated by the amplitude and angle values of the currents and voltages. On / off switches of various combinations of voltage and current sector are determined from the sector value. Based on the process, the ISVM technique can decrease switching losses in the power converter [26]. The ISVM utilizes a reference output voltage ($V_o^*$) and a reference input current ($I_i^*$) which are determined using the vector approach [27]. Equations (1)-(4) are used for the output voltage reference of the voltage source inverter.

$$V_o^* = d_a V_a + d_\beta V_\beta \quad (1)$$

$$d_a = \frac{T_a}{T_s} = m_V \sin(\frac{\pi}{3} - \theta_V) \quad (2)$$

$$d_\beta = \frac{T_\beta}{T_s} = m_V \sin(\theta_V) \quad (3)$$

$$0 \le m_V \le 1;\ m_V = \frac{\sqrt{3}V_o^*}{V_{DC}} \quad (4)$$

Where $d$ is the voltage duty cycle in $\alpha\beta$-axis, $V$ is the output voltage in $\alpha\beta$-axis, $m_V$ is the voltage modulation index, and $T_s$ is the switching time, $T_\alpha$ is the $\alpha$-axis time period and $T_\beta$ is the time period of $\beta$-axis. $\theta_V$ is the voltage sector angle. The reference input current of the current source rectifier are expressed in (5)-(8) [27].

$$I_i^* = d_\gamma I_\gamma + d_\delta I_\delta \quad (5)$$

$$d_\gamma = \frac{T_\gamma}{T_s} = m_C \sin(\frac{\pi}{3} - \theta_C) \quad (6)$$

$$d_\delta = \frac{T_\delta}{T_s} = m_C \sin(\theta_C) \quad (7)$$

$$0 \le m_C \le 1;\ m_C = \frac{I_i^*}{I_{DC}} \quad (8)$$

Where $d$ is the current duty cycle in $\gamma\delta$-axis, $I$ is the input current in $\gamma\delta$-axis, $m_C$ is the current modulation index, and $T_s$ is the switching time, $T_\gamma$ is the $\gamma$-axis time period and $T_\delta$ is the $\delta$-axis time period. $\theta_I$ is the current sector angle.

## 3. Fuzzy Supervisory Scalar Control

There are two methods of induction motor drives: scalar control and vector control. Scalar control is an interesting research issue because of its ease and robustness which can produce a minimum steady-state error. The scalar control does not require an induction motor model in electric driving, and so it is widely used in motor speed regulation without a decoupling process. Furthermore, conventional control systems have often been adopted by researchers to work in conjunction with the scalar control of three-phase induction motors because they are both proven to be effective techniques. The scalar method can be stated in (9) [28].

$$\Psi_m \cong \frac{V_p}{f} \cong K_v \quad (9)$$

where $\Psi_m$ is the magnetic field in the air gap, $V_p$ is the maximum voltage, and $K_v$ is the ratio of $V_p$ to frequency $f$.

The control method for producing constant v/f as given in (9) uses slip regulation that is illustrated in Figure 3. The reference speed ($\omega ref$) compared to actual speed ($\omega$). The result of the speed error ($e$), feeds to the speed control which can represent the converter voltage and frequency. FSC combined control is used as a speed controller. The slip value setting is needed so that the motor slip frequency does not exceed the limit of the motor operating quadrant. This way, it achieves stable operation close to the desired reference value and dynamic speed performance. The velocity error value is further used to represent the reference slip frequency ($\omega sl$). This $\omega sl$ signal is added to the actual motor speed ($\omega$) to determine the converter reference frequency ($f$). The branching of this signal enters the v/f ratio which results in the converter's reference voltage ($v$). The v/f ratio represents the voltage gain at low frequencies to keep the flux in the motor air gap constant.

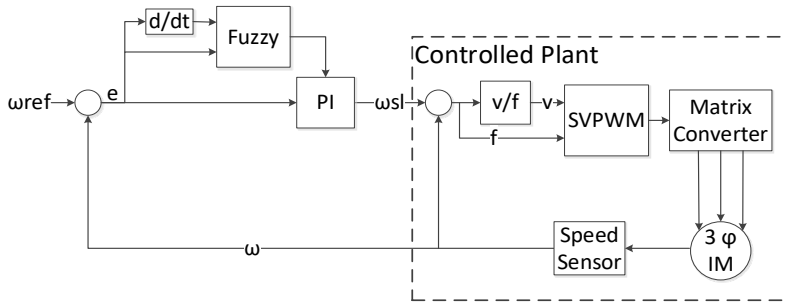


Figure 3. Diagram block Fuzzy Supervisory Scalar Control (FSSC) matrix converter drives a closed-loop system

Due to the physical construction of induction motors, their operation must follow certain operating standards which are typically labeled as their nominal ratings. These rating values must be considered when designing an induction motor drive. One such consideration is motor efficiency which in motor drives is strongly tied to the harmonic content of the system especially for operations outside the rating. Related to this, the choice of the motor drive control is important due to the direct impact on the level of harmonics or THD produced. This correlation is based

on the formulation of the rotor angular velocity ($\omega_r$) by modeling a three-phase induction motor which is shown (10) [29].

$$\frac{d\omega_r}{d\tau} = \frac{L_m}{JL_r}\left(\Psi_{r\alpha} i_{s\beta} - \Psi_{r\beta} i_{s\alpha}\right) - \frac{1}{J} t_o \quad (10)$$

In (10), one of the constituents for the rotor angular velocity ($\omega_r$) is determined from the stator current with $\alpha\beta$ reference frame. Meanwhile, the constituent components of the THD calculation consist of the sum of the current In values (in this case the stator current) which is shown in the (11) [30].

$$THD_I = \frac{\sqrt{\sum_{n=2}^{N} I_n^2}}{I_1} \quad (11)$$

The fuzzy logic controllers are frequently used as an alternate controller because of the ease with which they can represent the plant state to language or orally in managing and processing system information. Fuzzy logic controllers are also known for their reliability in overcoming systems with parameter uncertainties [31]. Additionally, since control complexity increases when used to control complex or non-linear systems, it is less efficient to design and tune controls manually. Hence, with the combined control of fuzzy logic and conventional control, the system can tune the controller automatically.

The input of the fuzzy logic controller is the difference in the reference speed and the speed sensor feedback ($e$) and the difference in the error value ($\Delta e$). The velocity error as a fuzzy input is kept at zero to equal the reference speed. Moreover, the process in fuzzy logic which consist of fuzzification, fuzzy rules, and defuzzification illustrated in Figure 4.

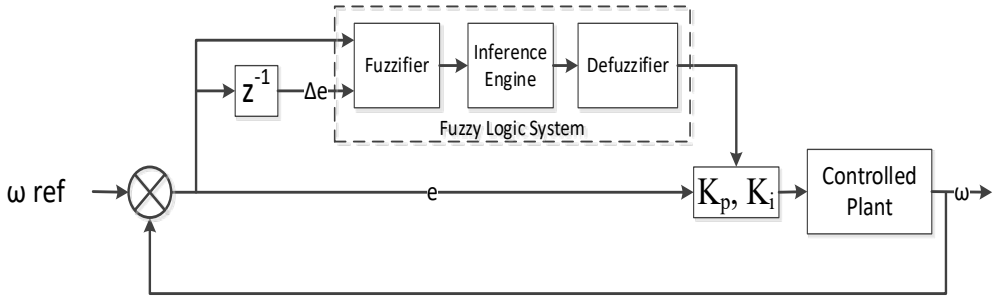


Figure 4. Fuzzy Supervisory Control Structure.

Input fuzzification or membership function (MF) has a vital role that determines the degree of membership for each state transition phase. The membership function is a curve that indicate the mapping of input data points into their membership values (often mentioned to as membership degrees) which have intervals between 0 and 1. Using seven triangular-shaped functions as input membership functions results in better detection of input states. Two inputs used are the error value ($e$) and the error change ($\Delta e$) for each of the corresponding output parameters $Kp$ and $Ki$. The triangle membership function converts these values into the corresponding fuzzy values.

The basic idea of the fuzzy inference system is to incorporate human knowledge into IF-THEN fuzzy set rules. The rules are defined after simulation and the fuzzy type Mamdani Inference Engine is used to map the input to the appropriate output. Furthermore, the input from the defuzzification process is a fuzzy set got from the configuration of fuzzy rules, while the resulting output is a number in the field of the fuzzy set.

The output side of $Kp$ uses the Gaussian function which is selected based on the functioning characteristics of its parameters. Defuzzification which converts the fuzzy output from the rule base into linguistic parameter values that affect the PI controller. The linguistic variables used are PS (Positive Small), PM (Positive Medium), PB (Positive Big), ZE (Zero Error), NB (Negative Big), NM (Negative Medium), and NS (Negative Small).

As a result, the fuzzy supervisor has the expert to determine and conclude the PI control

parameter effect values according to input conditions based on the rule-based inference system. Therefore, the PI control parameters can be more flexible referring to the error state that is zero. The MF fuzzy Mamdani type parameter design setting is based on the control algorithm shown in Figure 5, which has two inputs (($e$) and ($\Delta e$)) and two outputs (parameters of $Kp$ and $Ki$). The Fuzzy Inference System (FIS), membership function, and rules appearance are shown in Figure 6, respectively. All this works is done through MATLAB.

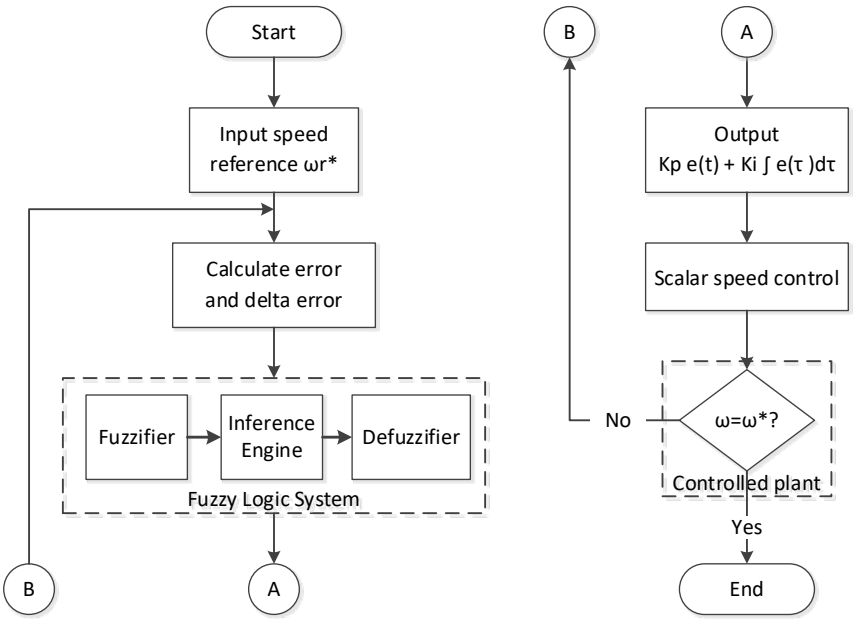


Figure 5. FSC Matrix Converter Diagram Block.

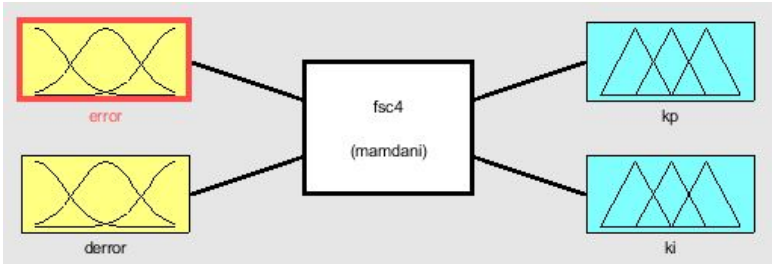


(a)

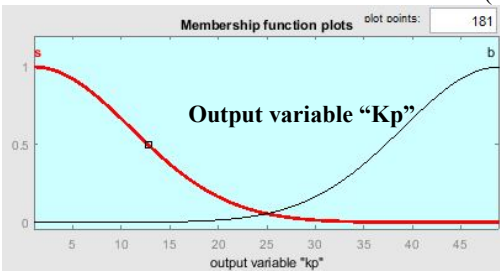


(b)

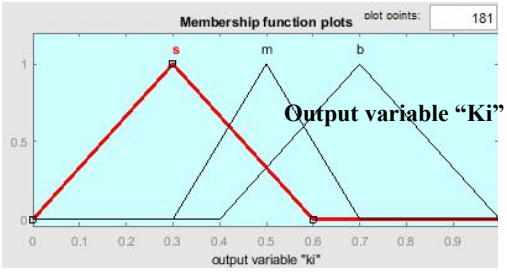


(c)

1. If (error is nm) and (derror is nm) then (kp is b)(ki is s) (1)
2. If (error is nb) and (derror is nm) then (kp is b)(ki is s) (1)
3. If (error is nb) and (derror is ns) then (kp is b)(ki is s) (1)
4. If (error is nb) and (derror is ze) then (kp is b)(ki is s) (1)
5. If (error is nb) and (derror is ps) then (kp is b)(ki is s) (1)
6. If (error is nb) and (derror is pm) then (kp is b)(ki is s) (1)
7. If (error is nb) and (derror is pb) then (kp is b)(ki is s) (1)
8. If (error is nm) and (derror is nb) then (kp is s) (1)
9. If (error is nm) and (derror is nm) then (kp is b) (1)
10. If (error is nm) and (derror is ns) then (kp is b)(ki is s) (1)
11. If (error is nm) and (derror is ze) then (kp is b)(ki is s) (1)
12. If (error is nm) and (derror is ps) then (kp is b)(ki is s) (1)
13. If (error is nm) and (derror is pm) then (kp is b) (1)
14. If (error is nm) and (derror is pb) then (kp is s) (1)
15. If (error is ns) and (derror is nb) then (kp is s)(ki is b) (1)
16. If (error is ns) and (derror is nm) then (kp is s) (1)
17. If (error is ns) and (derror is ns) then (kp is b) (1)
18. If (error is ns) and (derror is ze) then (kp is b)(ki is s) (1)
19. If (error is ns) and (derror is ps) then (kp is b) (1)
20. If (error is ns) and (derror is pm) then (kp is s) (1)
21. If (error is ns) and (derror is pb) then (kp is s)(ki is b) (1)
22. If (error is ze) and (derror is nb) then (kp is s)(ki is b) (1)
23. If (error is ze) and (derror is nm) then (kp is s)(ki is b) (1)
24. If (error is ze) and (derror is ns) then (kp is s) (1)
25. If (error is ze) and (derror is ze) then (kp is b) (1)
26. If (error is ze) and (derror is ps) then (kp is s) (1)
27. If (error is ze) and (derror is pm) then (kp is s)(ki is b) (1)
28. If (error is ze) and (derror is pb) then (kp is s)(ki is b) (1)
29. If (error is ps) and (derror is nb) then (kp is s)(ki is b) (1)
30. If (error is ps) and (derror is nm) then (kp is s) (1)
31. If (error is ps) and (derror is ns) then (kp is b) (1)
32. If (error is ps) and (derror is ze) then (kp is b)(ki is s) (1)
33. If (error is ps) and (derror is ps) then (kp is b) (1)
34. If (error is ps) and (derror is pm) then (kp is s) (1)
35. If (error is ps) and (derror is pb) then (kp is s)(ki is b) (1)
36. If (error is pm) and (derror is nb) then (kp is s) (1)
37. If (error is pm) and (derror is nm) then (kp is b) (1)
38. If (error is pm) and (derror is ns) then (kp is b)(ki is s) (1)
39. If (error is pm) and (derror is ze) then (kp is b)(ki is s) (1)
40. If (error is pm) and (derror is ps) then (kp is b)(ki is s) (1)
41. If (error is pm) and (derror is pm) then (kp is b) (1)
42. If (error is pm) and (derror is pb) then (kp is s) (1)
43. If (error is pb) and (derror is nb) then (kp is b)(ki is s) (1)
44. If (error is pb) and (derror is nm) then (kp is b)(ki is s) (1)
45. If (error is pb) and (derror is ns) then (kp is b)(ki is s) (1)
46. If (error is pb) and (derror is ze) then (kp is b)(ki is s) (1)
47. If (error is pb) and (derror is ps) then (kp is b)(ki is s) (1)
48. If (error is pb) and (derror is pm) then (kp is b)(ki is s) (1)
49. If (error is pb) and (derror is pb) then (kp is b)(ki is s) (1)

(d)

Figure 6. Fuzzy System (a) FIS Editor (b) Membership Function $Kp$ (c) Membership Function $Ki$ (d) Rules of FSC.

**4. Analysis**

As explained above, the 3x3 matrix converter drives without output filter were designed and modeled through computer simulation with parameters such as input voltage supply and motor capacity as shown in Table 1. Since the matrix converter is a direct AC–AC converter, the source waveform will greatly affect the output waveform especially when connected to a non-linear load such as a three-phase induction motor. Therefore, knowledge of how the matrix converter drive responds under three-phase source-side and load-side disturbances will be important to understand the complete operating behavior of the drive.

Source side disturbance in the form of unbalanced input voltage has been known to increase the THD levels in the input current and the output voltage of the motor drive converter. This occurs since additional frequency components beyond the fundamental component appear in the input current and output voltage waveforms as evident by the distortion of the waveform from the ideal sinusoidal shape. The presence of harmonics will further degrade the input power factor of the drive system. Therefore, evaluation of the impact of unbalanced source disturbance to THD input current ($THD_{Iin}$), output voltage ($THD_{Vout}$), and output current ($THD_{Iout}$) will also be important in understanding the operating behavior of the matrix converter for motor drive. As

part of this study, tests were carried out in a wide range of operating quadrants of the motor. In particular, tests that introduced a three-phase source with phase A under 10% nominal voltage, equivalent to the amplitude of 279.9 V, were conducted.

Table 1. System Parameters.

| Parameters | Values |
|---|---|
| Line-to-line input voltage ($Vll$) | 311 V |
| Frequency ($f$) | 50 Hz |
| Output power ($Pout$) | 4 kW |
| RMS voltage ($Vrms$) | 400 V |
| Stator resistance ($Rs$) | 1.405 Ω |
| Rotor resistance ($Rr$) | 1.395 Ω |
| Stator inductance ($Ls$) | 5.839 mH |
| Rotor inductance ($Lr$) | 5.839 mH |
| Number of pole pairs ($p$) | 2 |
| Mutual inductance ($Lm$) | 172.2 mH |
| Moment of inertia ($j$) | 0.0131 kg.m$^2$ |

The proposed system performance testing was then carried out by applying the following two conditions:

1. Dynamic speed (four-quadrant operation) with the unbalanced input voltage.
2. Constant speed with load-side disturbance and unbalanced input voltage.

For system performance comparison, simulation of the proposed system uses two controllers, PI controller and FSC. Speed measurement feedback from the speed sensor and setpoint is used as an input to both controllers. Figure 7 depicts the first case that looks at the dynamic speed response with unbalanced voltage disturbances in the four quadrants of motor operation. The test was simulated for 4 s during which a change in speed and operation of the motor was introduced at every 1 s interval.

To observe the dynamic operation of the drive, the forward acceleration starts from a stationary state until it reaches 1200 rpm (0 – 1 s) where the FSC has a lower overshoot value than that of the PI control with a difference of 7.17 %. To further evaluate the response, the forward motor operation was slowed down starting from 1200 rpm to 300 rpm (1 – 2 s) where the FSC yields a smaller undershoot than the PI control does. Likewise, in the reverse motoring operation, the speed is accelerated at -500 rpm (2 – 3 s) and the reverse operation is slowed down by -120 rpm (3 – 4 s), which results in the FSC overshoot value that is smaller than that of the PI control.

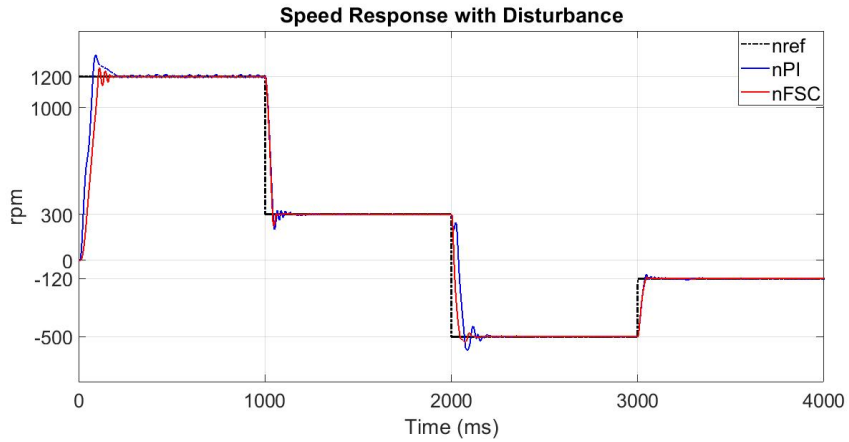


Figure 7. Four Quadrant Speed Response with Unbalanced Input Voltage Disturbance.

Unbalanced input voltage occurs when the network is connected with an unknown amount of nonlinear load. In addition, an unbalanced input voltage also occurs when there is a short circuit which results in distorted current and voltage waveforms [32]. Furthermore, the three-phase voltages from the grid supply in practice are likely to be unbalanced due to the uneven distribution of the loads. Figure 8 shows the input and output phase current responses when continuous unbalance input voltage is applied throughout the simulation time. The result shows that the initial percent overshoot and undershoot from the FSC is lower than that from the PI control.

Input current waveforms as depicted in Figure 8 (a) are observed to be stable due to the constant input frequency of 50 Hz. On the other hand, output current waveforms fluctuate in line with the changes in the output frequency, as shown in Figure 8 (b). When the steady-state is reached, the two controllers produce practically the same amplitude. Table 2 summarizes the responses and performance of the two PI controls and the FSC.

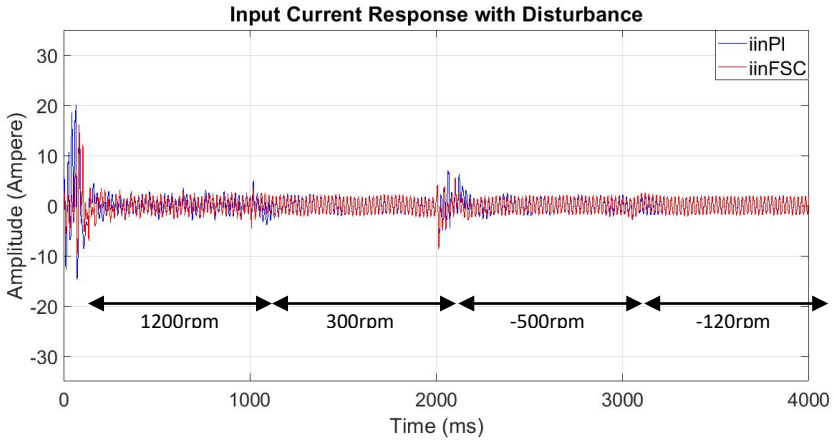


(a)

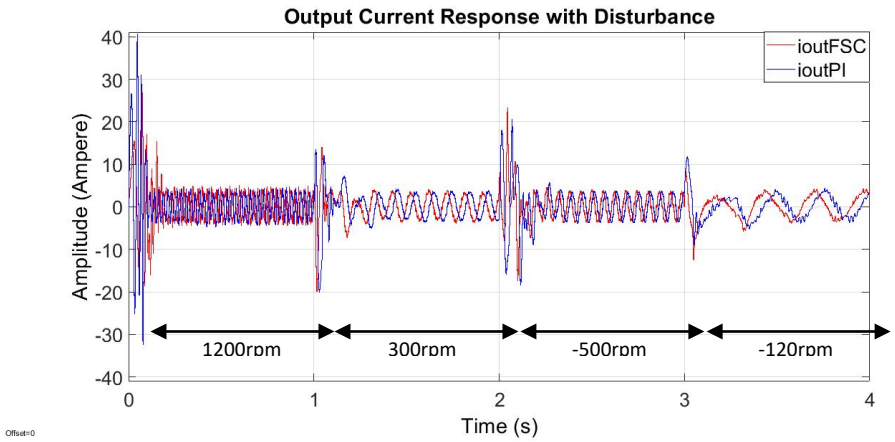


(b)

Figure 8. Four Quadrant Current Response with Disturbance (a) Input Current (b) Output Current.

Table 2. Dynamic Speed Performance in Four Quadrants of Motor Operation with Unbalanced Voltage Disturbance.

| Setpoint (rpm) | Overshoot (%) | | Rise Time (ms) | | Settling Time (ms) | | Error Steady State (%) | | Total Score Performance | |
|---|---|---|---|---|---|---|---|---|---|---|
| | FSC | PI | FSC | PI | FSC | PI | FSC | PI | FSC | PI |
| 1200 | 4.83 | 12.00 | 95.517 | 72.425 | 173.489 | 213.307 | 0 | 1.17 | 269.05 | 285.86 |
| 300 | 19.23 | 33.57 | 35.088 | 39.142 | 74.074 | 144.814 | 0 | 13.00 | 109.35 | 184.42 |
| -500 | 6.52 | 17.90 | 27.290 | 27.426 | 93.567 | 187.867 | 0 | 4.60 | 120.92 | 215.52 |
| -120 | 4.50 | 16.72 | 31.189 | 31.321 | 54.581 | 101.761 | 0 | 5.58 | 85.82 | 133.31 |

The second performance test was done with three-phase source-side and torque load-side disturbances. The test was carried out at a constant motor speed of 500 rpm. Figure 9 illustrates the constant speed test by adding a load torque disturbance of 20 Nm for 0.2 s (0.4 - 0.6 s). The system test is implemented in the nominal speed reference of the induction motor (1500 rpm) which has an impact on reducing the speed to 1465 rpm. The performance of the two controllers yields a graph with the same decrease in speed (35 rpm). For the performance of the induction motor load stator current, shown in Figures 9 (a) and 9 (b), the overshoot and undershoot percentage generated by the FSC has a lower value when compared with those from the PI control. However, when state steady is reached, the second controller has approximately the same amplitude as the higher FSC ripple.

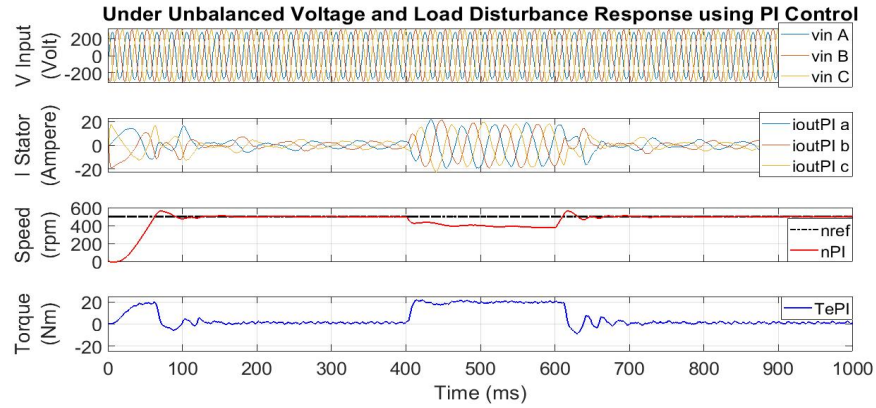


(a)

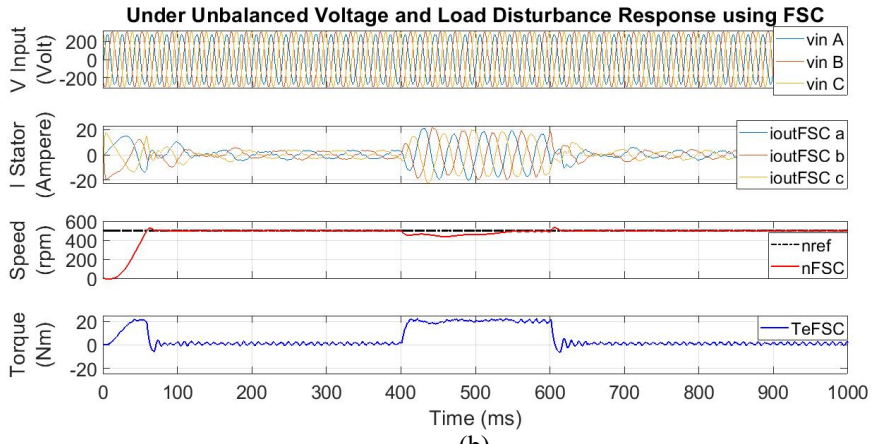


(b)

Figure 9. 500 rpm Constant Speed Performance with Load-sided 10 Nm and Unbalanced Voltage Disturbances (a) PI Control (b) FSC.

The high performance in speed and torque from the matrix converter drive is highly desirable since it will make the drive particularly suitable for improved industrial process control and high voltage applications such as large motors variable speed drives. Figure 9 shows balanced sinusoidal output currents are obtained that have the same phase with their corresponding input voltage as well as with the input current.
Figure 10 illustrates the comparison in the speed response produced by the two controllers. In the top graph, the FSC speed overshoot has a lower value when compared to the PI control. However, in the lower graph, the FSC torque ripple has more oscillation than the one resulted from the PI control.

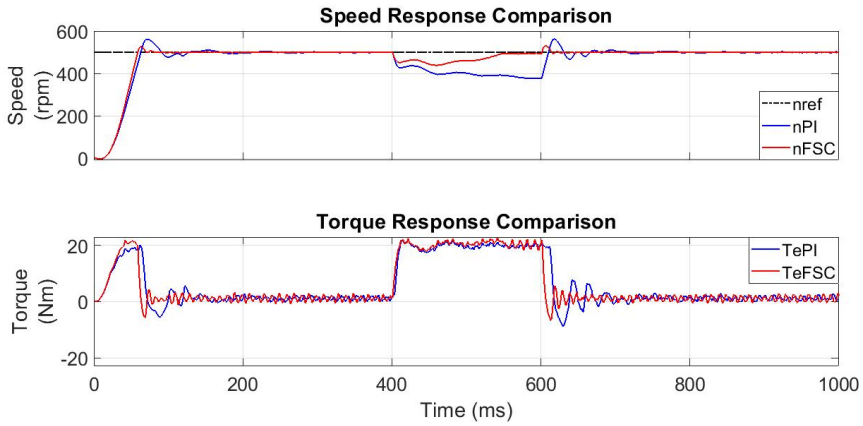


Figure 10. Detailed Comparison of Speed and Torque Responses of Two Controllers.

The PI controller used in the matrix converter - ISVM requires tuning the parameters for each speed setpoint change to get a satisfactory response. The other determining parameters for the performance comparison are the results of the THD value between the FSC and PI control which is shown in Table 4. The observed THD values came from the input current ($THD_{Iin}$), output current ($THD_{Iout}$), and output voltage ($THD_{Vout}$). The input voltage harmonics (($THD_{Vout}$) are not displayed because the system gets a voltage source for which the ideal frequency is 50 Hz. The THD value is observed at a constant low-speed setpoint which at this speed requires special treatment due to the torque-speed limit characteristics, the varying stator parameters, and poor motor performance [33].

Harmonic values represented by THD with three-phase source and load torque were observed at all times with unbalanced voltage and load disturbances (0.4–0.6 s) and afterload disturbance, but still with an unbalanced voltage source (0.7 - 1 s) to further evaluate the recovery response of the proposed controller. The THD performance evaluation is shown in Table 4, which shows that from 0.4 - 0.6 s FSC resulted in much lower harmonics than that of the PI control. Meanwhile, from 0.7 - 1 s, the THD from FSC was observed to be greater than that of PI control with the maximum difference of 4.31%.

Table 4. Evaluation of THD Value at 500 rpm Constant Speed with Load-sided 10 Nm and Unbalanced Voltage Disturbances.

| Condition | THD | | | | | |
|---|---|---|---|---|---|---|
| | *Iin* (%) | | *Iout* (%) | | *Vout* (%) | |
| | FSC | PI | FSC | PI | FSC | PI |
| Unbalanced | 11.38 | 9.43 | 19.87 | 15.56 | 9.71 | 8.53 |
| Unbalanced + Load disturbance | 49.76 | 50.43 | 369.32 | 653.48 | 402.69 | 740.86 |

## 5. Conclusion

Based on the results of performance tests conducted on the proposed motor drive system under various unbalanced voltage and load torque disturbances, the induction motor dynamic speed control has been achieved. The reference speed is set at dynamic and constant speeds with the source unbalanced condition was set with phase A voltage kept under 10% with concerning to the other two phases. Upon input and output disturbances, overshoot, undershoot, settling time, rise time, and steady-state error resulted from the FSC have lower values than those produced by the PI control. It was further noted that at the time of the disturbance, the Total Harmonic Distortion (THD) of the FSC matrix converter without filter output was better than the one resulting from the PI control. Based on the results of this study, the proposed FSC embedded in a scalar control matrix converter fed induction motor drive with Indirect Space Vector Modulation (ISVM) is a reliable speed control with minimum THD value and it has demonstrated its ability to mitigate the dynamic performance under the various input and output disturbances.

## 6. References


[1]. M. P. Jati, E. Purwanto, and B. Sumantri, "Comparative study of indirect space vector and venturini modulation for matrix converter fed induction motor," *J. Phys. Conf. Ser.*, vol. 1517, no. 1, pp. 1–8, 2020, doi: 10.1088/1742-6596/1517/1/012072.

[2]. Y. Mei and G. Yi, "A Self-tuning Method of Weighting Factor in Model Prediction Control for Indirect Matrix Converter with Induction Motor System," in *2019 22nd International Conference on Electrical Machines and Systems, ICEMS 2019*, 2019, pp. 1–5, doi: 10.1109/ICEMS.2019.8921450.

[3]. S. Tiwari and S. Rajendran, "Four Quadrant Operation and Control of Three Phase BLDC Motor for Electric Vehicles," in *2019 IEEE PES GTD Grand International Conference and Exposition Asia (GTD Asia)*, 2019, pp. 577–582.

[4]. W. Xiong *et al.*, "A Cost-Effective and Low-Complexity Predictive Control for Matrix Converters Under Unbalanced Grid Voltage Conditions," *IEEE Access*, vol. PP, no. c, pp. 1–12, 2019, doi: 10.1109/ACCESS.2019.2908446.

[5]. Y. Yan, H. An, T. Shi, and C. Xia, "Improved double line voltage synthesis of matrix converter for input current enhancement under unbalanced power supply," *IET Power Electron.*, vol. 6, no. 4, pp. 798–808, 2013, doi: 10.1049/iet-pel.2012.0588.

[6]. J. Zhang, L. Li, D. Dorrell, and Y. Guo, "Direct Torque Control with a Modified Switching Table for a Direct Matrix Converter based AC Motor Drive System," 2017, pp. 1–6.

[7]. T. Taufik, M. Muscarella, and D. Sawitri, "Power Quality Analysis of Variable Frequency Drives Connected to a Reactively Compensated Mixed Load System," in *International Seminar on Application for Technology of Information and Communication*, 2016, pp. 261–266.

[8]. M. Diaz *et al.*, "Vector Control of a Modular Multilevel Matrix Converter Operating over the Full Output Frequency Range," *IEEE Trans. Ind. Electron.*, vol. 66, no. 7, pp. 5102–5114, 2019.

[9]. M. Farhadi, M. T. Fard, and M. Abapour, "DC-AC Converter-Fed Induction Motor Drive with Fault-Tolerant Capability under Open- and Short-Circuit Switch Failures," *IEEE Trans. Power Electron.*, vol. 8993, no. c, pp. 1–13, 2017, doi: 10.1109/TPEL.2017.2683534.

[10]. L. Wang *et al.*, "A finite control set model predictive control method for matrix converter with zero common-mode voltage," *IEEE J. Emerg. Sel. Top. Power Electron.*, vol. 6, no. 1, 2018, doi: 10.1109/JESTPE.2017.2727501.

[11]. A. K. Singh and S. Pattnaik, "Matrix Converter Operated Hysteresis Current Controlled BLDC Motor Drive for Efficient Speed Control and Improved Power Quality," *Procedia Comput. Sci.*, vol. 167, no. 2019, pp. 541–550, 2020, doi: 10.1016/j.procs.2020.03.314.

[12]. M. Li, Y. Liu, and H. Abu-rub, "Optimizing Control Strategy of Quasi-Z Source Indirect Matrix Converter for Induction Motor Drives," 2017, pp. 1663–1668.

[13]. Y. Mei, L. Chen, and S. Wang, "Analysis on harmonic characteristic of the input current in indirect matrix converter," in *2017 20th International Conference on Electrical Machines and Systems, ICEMS 2017*, 2017, pp. 1–5, doi: 10.1109/ICEMS.2017.8055983.
[14]. M. Espinoza-b *et al.*, "An Integrated Converter and Machine Control System for MMC-Based High Power Drives," *IEEE Trans. Ind. Electron.*, vol. 0046, no. c, 2018, doi: 10.1109/TIE.2018.2801839.
[15]. J. Riedemann, R. Peña, R. Cárdenas, R. Blasco, and J. Clare, "Indirect Matrix Converter Modulation Strategies for Open-end Winding Induction Machine," *IEEE Lat. Am. Trans.*, vol. 12, no. 3, pp. 395–401, 2014.
[16]. M. Vijayagopal, L. Empringham, L. De Lillo, L. Tarisciotti, P. Zanchetta, and P. Wheeler, "Current Control and Reactive Power Minimization of a Direct Matrix Converter Induction Motor Drive with Modulated Model Predictive Control," 2015, pp. 103–108.
[17]. N. H. Viet, V. M. Hung, and N. Paraschiv, "FS-PTC with Switching Table for Matrix Converter in Induction Motors Drive System," in *2019 International Symposium on Electrical and Electronics Engineering (ISEE)*, 2019, pp. 298–303.
[18]. M. Raghuram, A. K. Chauhan, and S. K. Singh, "Extended Range of Ultra Sparse Matrix Converter using Integrated Switched Capacitor Network," *IEEE Trans. Ind. Appl.*, vol. PP, no. c, p. 1, 2019, doi: 10.1109/TIA.2019.2928285.
[19]. J. Kang, H. Hara, E. Yamamoto, and E. Watanabe, "Analysis and Evaluation of Bi-Directional Power Switch Losses for Matrix Converter Drive," in *IEEE Industry Application Conference*, 2002, pp. 438–443.
[20]. M. Su *et al.*, "Modified modulation scheme for three-level diode-clamped matrix converter under unbalanced input conditions," *IET Power Electron.*, pp. 1–9, 2018, doi: 10.1049/iet-pel.2017.0512.
[21]. E. Purwanto, M. P. Jati, B. Sumantri, and M. R. Rusli, "Performance Enhancement of Matrix Converter Fed Induction Motor Drives Using Fuzzy Supervisory Controller," in *International Electronics Sysmposium*, 2020, pp. 60–66.
[22]. M. Rivera, P. Wheeler, A. Olloqui, and D. A. Khaburi, "A review of predictive control techniques for matrix converters-Part i," in *7th Power Electronics, Drive Systems and Technologies Conference, PEDSTC 2016*, 2016, doi: 10.1109/PEDSTC.2016.7556925.
[23]. R. Vargas, M. Rivera, J. Rodriguez, and P. Wheeler, "Torque and Flux Control of an Induction Machine fed by a Matrix Converter under Unbalanced AC Supply with Reactive Power Minimization," 2015, pp. 441–446.
[24]. R. N. Hasanah, R. Ramadhan, H. Suyono, and T. Taufik, "Performance Study of PID and Voltage Mode Controllers in Voltage Regulator for," in *International Conference on Computional Science and Computional Intelligence*, 2019, pp. 732–737, doi: 10.1109/CSCI49370.2019.00139.
[25]. P. W. Wheeler, "Matrix Converters : A Technology Review," *IEEE Trans. Ind. Electron.*, vol. 49, no. 1, pp. 1–5, 2014, doi: 10.1007/s13398-014-0173-7.2.
[26]. Q. Guan, P. Wheeler, O. Simon, Q. Guan, and J. Clare, "Geometrical visualisation of indirect space vector modulation for matrix converters operating with abnormal supplies," *IET Power Electron.*, pp. 1–11, 2019, doi: 10.1049/iet-pel.2019.0406.
[27]. S. Arya and G. K. Nisha, "Indirect Space Vector Modulation Based Three Phase Matrix Converter," in *IEEE International Conference on Control, Communication, and Computing*, 2018, pp. 68–73.
[28]. B. S. S. G. Yelamarthi and S. R. Sandepudi, "Scalar Control of Induction Motor Drive with Inverter Fault-Tolerance Capability," in *IEEE International Conference on Emerging Frontiers in Electrical and Electronic Technologies (ICEFEET)*, 2020, pp. 1–5.
[29]. D. C. Happyanto, A. W. Aditya, and B. Sumantri, "Boundary – Layer Effect in Robust Sliding Mode Control for Indirect Field Oriented Control of 3-Phase Induction Motor," *Int. J. Electr. Informatics*, vol. 12, no. 2, pp. 188–204, 2020, doi: 10.15676/ijeei.2020.12.2.2.
[30]. E. D. Baranov, V. I. Popov, and R. I. Yakimov, "An Analysis of Input and Output THD Factors of Matrix Converter," in *IEEE International Conference of Young Specialists on*

*Micro/Nanotechnologies and Electron Devices (EDM)*, 2018, pp. 6403–6406.
[31]. T. Ramesh, A. K. Panda, and S. S. Kumar, "Fuzzy Logic and Sliding-Mode Speed Control Based Direct Torque and Flux Control Scheme to Improve the Performance of an Induction Motor Drive," *Int. J. Electr. Informatics*, vol. 6, no. 1, pp. 155–180, 2014.
[32]. X. Wang, H. Lin, H. She, and B. Feng, "A Research on Space Vector Modulation Strategy for Matrix Converter Under Abnormal Input-Voltage Conditions," *IEEE Trans. Ind. Electron.*, vol. 59, no. 1, pp. 93–104, 2012.
[33]. T. N. Mir, B. Singh, and A. H. Bhat, "Low Speed Sensorless Model Predictive Current Control of a Three Phase Induction Motor from a Single Phase Supply," in *2018 IEEMA Engineer Infinite Conference (eTechNxT)*, 2018, pp. 1–6.

**Mentari Putri Jati** currently is a lecturer in Universitas Negeri Yogyakarta. She received her master (2020) and bachelor degree (2018) in electrical engineering from Politeknik Elektronika Negeri Surabaya. Her research interests are related to electric drives, electric machine, power electronics, control system, and renewable energy.

**Era Purwanto** was born in Surabaya, Indonesia on June 1, 1961. He completed his bachelor's degree in Institut Teknologi Sepuluh Nopember. Then continued his Master's education at Shizuoka University, Japan. He completed the master's program in 1995. Then continued his study and got a Doctor in 2013. He was joined Politeknik Elektronika Negeri Surabaya, Indonesia in 1987 as lecture. His love in the concentration of the Power Systems Engineering, made the author do a lot of research and publicize both journals and seminars in the field of Power Systems Engineering.

**Bambang Sumantri** is a lecturer of Politeknik Elektronika Negeri Surabaya (PENS), Indonesia. He received bachelor degree in Electrical Engineering from Institut Teknologi Sepuluh Nopember (ITS), Indonesia, in 2002, M.Sc (Master of Science) in Control Engineering from Universiti Teknologi Petronas, Malaysia, in 2009, and Doctor of Engineering in Mechanical Engineering, Toyohashi University of Technology, Japan, in 2015. His research interest is in robust control system, robotics, and embedded control system.

**Muhammad Rizani Rusli** was born in Sidoarjo, Indonesia on December 22, 1995. He is currently a research and development engineer of PT. Garda Energi Nasional Indonesia in Sidoarjo, Indonesia. He received his bachelor and master degree in electrical engineering from Politeknik Elektronika Negeri Surabaya (PENS) in 2017 and 2019. He has experience as a research engineer in Pusat Unggulan IPTEK Perguruan Tinggi (PUI-PT)– Sistem dan Kontrol Otomotif, Institut Teknologi Sepuluh Nopember, Surabaya, Indonesia (2017-2020). His research interests are related to power electronics, electric drives, electric machines, and control system.

**Aris Nasuha** is a lecturer in the Department of Electronics and Informatics Engineering Education, Universitas Negeri Yogyakarta. He received a bachelor degree in Pyschics from Universitas Gadjah Mada Yogyakarta (1993), a master degree in Control System Engineering from Institut Teknologi Sepuluh Nopember Surabaya (2001), and a PhD degree in Electrical Engineering from Institut Teknologi Sepuluh Nopember Surabaya (2019). His research interest include intelligenct control, digital image processing and artificial intelligence.

**Anang Tjahjono** was born on November 19, 1964 in Ponorogo, East Java, Indonesia. Graduated from the master's program in 1999 and graduated from a doctoral program in 2020 from Institut Teknologi Sepuluh Nopember, Indonesia. Currently conducting research on the implementation of artificial intelligence in the field of smart electricity networks and control systems. Starting in 1990 as a lecturer at Politeknik Elektronika Negeri Surabaya, Indonesia, currently doing various research collaborations with industry.

**Taufik** received his BS in Electrical Engineering with minor in Computer Science from Northern Arizona University, MS in Electrical Engineering from University of Illinois Chicago, and Doctor of Engineering from Cleveland State University. He joined the Electrical Engineering department at Cal Poly State University in 1999 where he is currently a tenured Full Professor and the Director of Electric Power Institute. He received numerous teaching awards, most notably the 2012 Outstanding Teaching Award from the American Society of Engineering Education - Pacific Southwest Section. He is a Senior Member of IEEE and has industry experience with several companies including Capstone Microturbine, Rockwell Automation, Picker International, San Diego Gas & Electric, APD Semiconductor, Diodes Inc., Enerpro, Renewable Power Conversion and Sempra Energy. His areas of research include power electronics, power systems, rural electrification, energy harvesting, renewable energy and smart grid. He has published over 200 technical papers and journals, reports, books, course readers, and served on the editorial review boards of several journals.